JOURNAL OF COMPUTATIONAL PHYSICS 34, 371–389 (1980)

Finite Elements Incorporating Characteristics for One-Dimensional Diffusion–Convection Equation

EROL VAROĞLU

Faculty of Graduate Studies, The University of British Columbia, Civil/Mechanical Engineering Bldg., Room 2006, Vancouver, British Columbia V6T 1W5, Canada

AND

W. D. LIAM FINN

Faculty of Graduate Studies and Department of Civil Engineering, The University of British Columbia, Civil/Mechanical Engineering Bldg., Room 2004, Vancouver, British Columbia V6T 1W5, Canada

Received January 19, 1979; revised May 30, 1979

A finite element method incorporating the method of characteristics for the solution of diffusion–convection equation with variable coefficients in one spatial dimension is developed. The method employs spatial–temporal elements with sides joining the nodes at subsequent time levels oriented in particular directions. This method is capable of solving diffusion–convection equation accurately for the whole spectrum of dispersion from pure diffusion, through mixed dispersion, to pure convection in particular, employing any mesh of reasonable size. The application of the method is demonstrated by solving three examples.

1. INTRODUCTION

Analysis of the transport of pollutants in lakes, channels, in near shore zones and in surface and subsurface hydrology, requires the numerical solution of the diffusion–convection equation.

Most of the numerical solutions of the diffusion–convection equation are based on finite differences in space and time (Price *et al.* [18], Chaudhari [4], Keller [12], Book *et al.* [3], and Martin [14]) or a combination of Galerkin type finite elements in space and finite differences in time (Price *et al.* [17], Adey and Brebbia [1], Dailey and Harleman [6], and Smith *et al.* [20]).

A review and comparison of the numerical methods for the solution of the diffusion–convection equation can be found in papers by Lam [13], Ehlig [7], van Genuchten [21], Mercer and Faust [15], and Smith [19]. These studies show that most of the numerical methods give satisfactory numerical results for diffusion dominated flow problems, however, when convection is a strong component of dispersion, the existing numerical techniques have an intrinsically unstable character which exhibits

0021-9991/80/030371–19$02.00/0

oscillations, overshooting, numerical diffusion, negative concentrations, and clipping errors even in one-dimensional dispersion problems.

It is shown by Mercer and Faust [15] that reduction of the integration time step or reduction of the space increment is not sufficient to eliminate oscillations in conventional finite element solutions of some immiscible flow problems. Neither higher order finite elements (van Genuchten [21]), nor higher order integration schemes in time (Smith [19]) eliminate oscillations and overshooting in convection dominated flow problems.

Numerical examples given by Lam [13] show that the central differencing scheme and box scheme are oscillatory; upstream differencing introduces large artificial diffusion and when flux correction is used to control oscillations in upstream differencing schemes, sharp concentration fronts are smeared and clipping errors are created even in one-dimensional convection dominated flows.

In this paper, a new finite element method has been developed which, in each limiting case, reduces to an efficient, stable solution procedure for either pure convection or pure diffusion problems. The method employs a combination of linear triangular and four node isoparametric trapezoidal space–time finite elements. An extensive study of isoparametric finite elements is given by Oden [16] and Zienkiewicz [22]. Linear triangular space–time elements are employed by Oden [16] to solve wave equation in one spatial dimension. Also, isoparametric trapezoidal space–time elements have been used to solve free boundary problems associated with the heat equation (Bonnerot and Jamet [2], Jamet [11]) and to solve the systems of equations representing conservation laws (Jamet and Bonnerot [10], Jamet [11]). In the proposed method, stability is achieved by incorporating the method of characteristics into the finite element method. In the case of pure diffusion, the method reduces to the finite element method given by Gray and Pinder [8] for the diffusion equation. Since the method reduces to the method of characteristics in the case of pure convection, it is also very efficient and accurate for convection dominated flow problems.

The derivation of the method is given here for the one-dimensional diffusion–convection equation with variable coefficients. The utility and accuracy of the method are illustrated by application to several examples.

2. Statement of the Problem

The method of solution will be developed for the diffusion–convection equation in one spatial dimension x and time t given as

$$s(x)\frac{\partial C}{\partial t} = \frac{\partial}{\partial x}\left[D(x,t)\frac{\partial C}{\partial x} - u(x,t)C\right] - q(x,t)C, \qquad x_L < x < x_R, \quad t > 0, \tag{1}$$

where s, D, u, q are given and $C(x,t)$ is sought. It is assumed that $s(x) \neq 0$ for $x_L \leqslant x \leqslant x_R$. In the following analysis, $s(x) > 0$ for $x_L \leqslant x \leqslant x_R$ is assumed without losing any generality. For transport problems in surface hydrology, $s = 1$

and C, D, u, q denote solute concentration, dispersion coefficient, mass average velocity, and decay coefficient, respectively. In the case of transport through a saturated porous medium s is the retardation factor, and seepage velocity is denoted by u.

The initial condition can be expressed as

$$C(x, 0) = f(x), \qquad x_L < x < x_R . \tag{2}$$

The boundary conditions are taken as

$$C(x_L , t) = c_L(t), \qquad t > 0, \tag{3}$$

$$C(x_R , t) = c_R(t), \qquad t > 0. \tag{4}$$

The modifications necessary for the type of boundary conditions for which $\partial C/\partial x$ is prescribed will be discussed later.

In the case of pure convection $D = 0$, and in this case, both boundary conditions (Eqs. (3) and (4)) can be prescribed if $u(x_L , t) > 0$ and $u(x_R , t) < 0$.

3. The Method of Solution

3.1. *The Method of Weighted Residuals*

The method of weighted residuals will be employed to solve Eqs. (1)–(4). The notation used by Bonnerot and Jamet [2] will be adopted with slight modifications throughout the paper. Let $\hat{c}(x, t)$ be an approximation to the solution $C(x, t)$ of Eqs. (1)–(4). The vanishing of the weighted residual of Eq. (1) with respect to a continuous function $\phi(x, t)$ defined in $x_L \leqslant x \leqslant x_R$, $\tau_1 \leqslant t \leqslant \tau_2$ can be expressed as

$$\int_{\tau_1}^{\tau_2} \int_{x_L}^{x_R} \left[s \frac{\partial \hat{c}}{\partial t} - \frac{\partial}{\partial x} \left(D \frac{\partial \hat{c}}{\partial x} \right) + \frac{\partial}{\partial x} (u\hat{c}) + q\hat{c} \right] \phi \, dx \, dt = 0, \qquad 0 \leqslant \tau_1 < \tau_2 . \tag{5}$$

Employing integration by parts, Eq. (5) becomes

$$\int_{\tau_1}^{\tau_2} \int_{x_L}^{x_R} \left(-s\hat{c} \frac{\partial \phi}{\partial t} + D \frac{\partial \hat{c}}{\partial x} \frac{\partial \phi}{\partial x} - u\hat{c} \frac{\partial \phi}{\partial x} + q\hat{c}\phi \right) dx \, dt$$

$$+ \int_{x_L}^{x_R} \{ s\hat{c}\phi \}_{t=\tau_1}^{\tau_2} \, dx - \int_{\tau_1}^{\tau_2} \left\{ D \frac{\partial \hat{c}}{\partial x} \phi - u\hat{c}\phi \right\}_{x=x_L}^{x_R} dt = 0. \tag{6}$$

In the last two line integrals brackets are used for brevity to denote

$$\{ \psi(x_1 , x_2) \}_{x_i=a}^{b} = \psi(b, x_2) - \psi(a, x_2), \qquad i = 1,$$

$$= \psi(x_1 , b) - \psi(x_1 , a), \qquad i = 2. \tag{7}$$

In the following analysis, it is assumed that $u(x_L, t) > 0$ and $u(x_R, t) > 0$. This assumption facilitates the presentation of the fundamental ideas of the proposed method by means of a concrete case. The modifications required in the analysis are discussed in Section 3.5 if the velocity field violates the above assumptions.

The problem will be solved step by step in time employing finite elements in space and time. Let $\tau_1 = t^n$ and $\tau_2 = t^{n+1}$ denote the beginning and the end of a typical time step n. The domain of integration $x_L < x < x_R$, $t^n \leqslant t \leqslant t^{n+1}$ will be discretized by the spatial-temporal elements $K_0^n, K_1^n, \ldots, K_{I-1}^n$ as illustrated in Fig. 1.

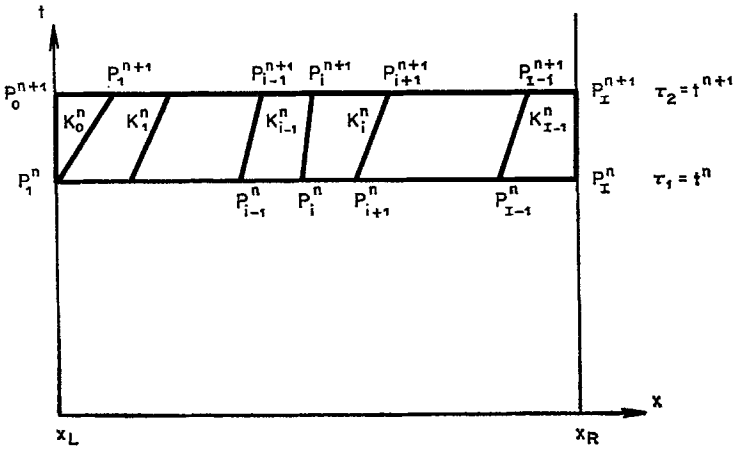

FIG. 1. Finite elements in space and time at a typical time step.

At a typical time step, we consider two types of elements, triangular and trapezoidal. A triangular element is required next to the left hand boundary in order to permit a finite element formulation which incorporates the characteristics of this problem as will be explained in Section 3.3.

3.2. *Finite Element Approximation*

Let c_j^m denote the value of the approximating function $\hat{c}$ at the node P_j^m. At each time step, either the initial values of the approximating function $c_1^n, c_2^n, \ldots, c_I^n$ are determined by the solution at the previous time step ($n > 0$) or imposing the condiiton that $\hat{c}$ satisfies the initial condition given by Eq. (2), ($n = 0$),

$$c_i^0 = f(x_i), \qquad i = 1, 2, \ldots, I. \tag{8}$$

In order to derive the finite element approximation to Eq. (6) the trapezoidal finite elements are transformed from the x–t global co-ordinate system to an η–ξ local co-ordinate system such that the transformed element in the η–ξ system is a unit square ($0 \leqslant \eta \leqslant 1$, $0 \leqslant \xi \leqslant 1$). The procedure was developed by Bonnerot and Jamet [2] and is summarized here. The co-ordinate transformation which maps a

unit square to the typical trapezoidal element, K_i^n, in the x–t plane can be expressed as

$$t = t^n + \xi(t^{n+1} - t^n), \tag{9}$$

$$x = (1 - \eta)[(1 - \xi)\, x_i^n + \xi x_i^{n+1}] + \eta[(1 - \xi)\, x_{i-1}^n + \xi x_{i-1}^{n+1}]. \tag{10}$$

The Jacobian of this transformation is

$$J_i^n = k(x_{i-1}^{n+\xi} - x_i^{n+\xi}) \tag{11}$$

in which

$$k = t^{n+1} - t^n, \tag{12}$$

$$x_i^{n+\xi} = (1 - \xi)\, x_i^n + \xi x_i^{n+1}, \tag{13}$$

and x_j^m denotes the x-coordinate of the point P_j^m in the x–t plane. In the local co-ordinates, the approximate solution over a typical trapezoidal element K_i^n will be taken as a polynomial of the form

$$\hat{c}(\eta, \xi) = (1 - \eta)(1 - \xi)\, c_i^n + (1 - \eta)\, \xi c_i^{n+1} + \eta(1 - \xi)\, c_{i-1}^n + \eta\xi c_{i-1}^{n+1}. \tag{14}$$

It is clear that $\hat{c}(x, t)$ is linear along each side of the trapezoid K_i^n. Since the shape functions used in Eq. (14) are also used in the coordinate transformation, Eqs. (9), (10), the finite elements are isoparametric.

Similarly, $C(x, t)$ in the triangular element K_0^n, is approximated by the polynomial

$$\hat{c}(\eta', \xi) = (1 - \eta')\, c_0^{n+1} + (1 - \xi)\, c_1^n + (\eta' + \xi - 1)\, c_1^{n+1} \tag{15}$$

in the local co-ordinates $(\eta' - \xi)$ where η' is defined as

$$\eta' = 1 + (x - x_1^{n+\xi})/(x_1^{n+1} - x_0^{n+1}) \tag{16}$$

with $x_1^{n+\xi}$ and ξ given by Eqs. (13) and (9), respectively.

The requirement that the approximate solution $\hat{c}$ should satisfy the boundary conditions, Eqs. (3), (4), yields

$$c_0^{n+1} = c_L(t^{n+1}), \tag{17}$$

$$c_I^{n+1} = c_R(t^{n+1}). \tag{18}$$

Since the nodal values c_i^n $(i = 1, 2, \ldots, I)$ are prescribed for $n = 0$ or are evaluated at the previous time step for $n > 0$ and therefore are known, there is one unknown for each internal node $(c_i^{n+1},\ i = 1, 2, \ldots, I - 1)$ to be evaluated at each time step. The boundary values of the approximating function c_0^{n+1} and c_I^{n+1} are known (Eqs. (17) and (18)).

Let the space V denote the space of all the continuous functions defined on the finite elements, K_0^n by Eq. (15) and K_1^n, K_2^n, ..., K_{I-1}^n by Eq. (14). A function ϕ in V is uniquely determined by its values at all the nodes P_i^n $(i = 1, 2, \ldots, I)$ and P_i^{n+1}

$(i = 0, 1,..., I)$, and is linear along the sides of the finite elements. We define the weighting function $\phi(x, t)$ for each i $(i = 1, 2,..., I - 1)$ as the function of space V such that

$$\begin{aligned} \phi^{(i)}(P_j^{n+1}) &= 1, \quad i = j \text{ or } i = 1, j = 0 \text{ or } i = I - 1, j = I \\ &= 0, \quad \text{otherwise} \qquad\qquad j = 0, 1,..., I \\ & \qquad\qquad\qquad\qquad\quad i = 1, 2,..., I - 1. \\ \phi^{(i)}(P_j^{n}) &= 1, \quad i = j \text{ or } i = I - 1, j = I \\ & \qquad\qquad\qquad\qquad\quad j = 1, 2,..., I \\ &= 0, \quad \text{otherwise.} \end{aligned} \tag{19}$$

The weighting functions defined over trapezoidal elements are the same as that successfully employed by Jamet and Bonnerot [10] for a system of conservation laws. Replacing $\phi(x, t)$ by $\phi^{(i)}$ $(i = 1, 2,..., I - 1)$ in Eq. (6) and taking $\tau_1 = t^n$ and $\tau_2 = t^{n+1}$, $I - 1$ equations in the unknowns c_i^{n+1}, $i = 1, 2,..., I - 1$ are obtained as follows:

$$\sum_{j=0}^{I-1} \iint_{K_j^n} \left(-s\hat{c}\frac{\partial \phi^{(i)}}{\partial t} + D\frac{\partial \hat{c}}{\partial x}\frac{\partial \phi^{(i)}}{\partial x} - u\hat{c}\frac{\partial \phi^{(i)}}{\partial x} + q\hat{c}\phi^{(i)}\right) dx\, dt$$

$$+ \int_{x_L}^{x_R} \{s\hat{c}\phi^{(i)}\}_{t=t^n}^{t^{n+1}} dx - \int_{t^n}^{t^{n+1}} \left\{D\frac{\partial \hat{c}}{\partial x}\phi^{(i)} - u\hat{c}\phi^{(i)}\right\}_{x=x_L}^{x_R} dt = 0,$$

$$i = 1, 2,..., I - 1. \tag{20}$$

It should be noted that

$$\sum_{i=1}^{I-1} \phi^{(i)} = 1, \qquad t^n \leqslant t \leqslant t^{n+1}, \qquad x_L \leqslant x \leqslant x_R\,. \tag{21}$$

Thus, the approximate solution $\hat{c}$ which satisfies Eq. (20) also satisfies the conservation relation

$$\int_{t^n}^{t^{n+1}} \int_{x_L}^{x_R} \left[s\frac{\partial \hat{c}}{\partial t} - \frac{\partial}{\partial x}\left(D\frac{\partial \hat{c}}{\partial x}\right) + \frac{\partial}{\partial x}(u\hat{c}) + q\hat{c}\right] dx\, dt = 0 \tag{22}$$

at each time step. The conservation relation in Eq. (22) can be reduced to the conservation relation given by Jamet and Bonnerot [10] in the case of a single hyperbolic equation. For brevity, we define A_i, $L_{n,i}$ and $L_{\bar{x}}$ as

$$A_i(\psi) = \int_{K_{i-1}^n + K_i^n} \psi(x, t)\, dx\, dt, \tag{23}$$

$$L_{n,i}(\psi) = \int_{x_i^n}^{x_{i+1}^n} \psi(x, t^n)\, dx, \tag{24}$$

$$L_{\bar{x}}(\psi) = \int_{t^n}^{t^{n+1}} \psi(\bar{x}, t)\, dt \tag{25}$$

for an arbitrary continuous function ψ defined on the domain of integration of each integral. Then, non-vanishing element contributions to Eq. (20) yield

$$
\begin{aligned}
&-A_i\left(s\hat{c}\frac{\partial\phi^{(i)}}{\partial t}\right)+A_i\left(D\frac{\partial\hat{c}}{\partial x}\frac{\partial\phi^{(i)}}{\partial x}\right)-A_i\left(u\hat{c}\frac{\partial\phi^{(i)}}{\partial x}\right)+A_i(q\hat{c}\phi^{(i)})\\
&\quad+L_{n+1,i-1}(s\hat{c}\phi^{(i)})+L_{n+1,i}(s\hat{c}\phi^{(i)})-L_{n,i-1}(sc\phi^{(i)})\\
&\quad-L_{n,i}(sc\phi^{(i)})+\delta_{i,1}\left[L_{x_L}\left(D\frac{\partial\hat{c}}{\partial x}\phi^{(1)}\right)-L_{x_L}(u\hat{c}\phi^{(1)})\right]\\
&\quad-\delta_{i,I-1}\left[L_{x_R}\left(D\frac{\partial\hat{c}}{\partial x}\phi^{(I-1)}\right)-L_{x_R}(u\hat{c}\phi^{(I-1)})\right]=0, \qquad i=1,2,\ldots,I-1
\end{aligned}
\tag{26}
$$

where

$$
\delta_{i,j}=\begin{cases}1, & i=j\\ 0, & i\neq j\end{cases}
\qquad
L_{n,0}(s\hat{c}\phi^{(1)})=0.
$$

The area integral over the triangular element is approximated as

$$
\iint_{K_0''}\psi\,dx\,dt\simeq\frac{1}{6}k(x_1^{n+1}-x_0^{n+1})[\psi(P_1^{\,n})+\psi(P_0^{n+1})+\psi(P_1^{n+1})] \tag{27}
$$

and 2×2 points Newton–Cotes quadrature

$$
\iint_{K_i^n}\psi\,dx\,dt\simeq\frac{1}{4}\sum_{\xi=0}^{1}\sum_{\eta=0}^{1}\psi(P_{i+\eta}^{n+\xi})\,J_i^n(\xi), \qquad i=1,2,\ldots,I-1, \tag{28}
$$

is employed to evaluate the area integrals over trapezoidal elements. The line integrals are approximated by using trapezoidal rule. For brevity, $\psi(P_j^m)$ will be denoted by ψ_j^m where $\psi(x,y)$ is an arbitrary continuous function defined at the point $P_j^m(x_j^m, t^m)$. The explicit expressions for each term in Eq. (26) are given in Tables I and II.

3.3. *Characteristics in Finite Elements*

Difficulties arise in existing numerical methods when convection is the dominant factor in dispersion. When $D=0$, the partial differential equation, Eq. (1), reduces to

$$
s(x)\frac{\partial C}{\partial t}+u(x,t)\frac{\partial C}{\partial x}=-\left[q(x,t)+\frac{\partial u}{\partial x}\right]C. \tag{29}
$$

Along the characteristic curves of this first order partial differential equation we have (Hildebrand [9])

$$
\frac{dx}{u(x,t)}=\frac{dt}{s(x)}=-\frac{dC}{[q(x,t)+\partial u/\partial x]C}. \tag{30}
$$

These equations represent two families of integral surfaces of Eq. (29). A character-

TABLE I

Finite element contributions	$i = 1$	$i = 2, 3, \ldots, I-2$	$i = I-1$
$A_i\left(s\hat{c}\,\frac{\partial\phi^{(i)}}{\partial t}\right)$	$\frac{1}{4}[(x_1^{n+1}-x_1^n)(s_1^n c_1^n+s_1^{n+1}c_1^{n+1})$ $+(x_2^{n+1}-x_2^n)(s_2^n c_2^n+s_2^{n+1}c_2^{n+1})]$	$\frac{1}{4}[(x_{i+1}^{n+1}-x_{i+1}^n)(s_{i+1}^n c_{i+1}^n+s_{i+1}^{n+1}c_{i+1}^{n+1})$ $-(x_{i-1}^{n+1}-x_{i-1}^n)(s_{i-1}^n c_{i-1}^n+s_{i-1}^{n+1}c_{i-1}^{n+1})]$	$-\frac{1}{4}[(x_{I-2}^{n+1}-x_{I-2}^n)(s_{I-2}^n c_{I-2}^n+s_{I-2}^{n+1}c_{I-2}^{n+1})$ $+(x_{I-1}^{n+1}-x_{I-1}^n)(s_{I-1}^n c_{I-1}^n+s_{I-1}^{n+1}c_{I-1}^{n+1})]$
$A_i\left(D\,\frac{\partial\hat{c}}{\partial x}\,\frac{\partial\phi^{(i)}}{\partial x}\right)$	$-\frac{k}{4}\left[(D_2^n+D_1^n)\,\frac{c_2^n-c_1^n}{x_2^n-x_1^n}\right.$ $\left.+(D_2^{n+1}+D_1^{n+1})\,\frac{c_2^{n+1}-c_1^{n+1}}{x_2^{n+1}-x_1^{n+1}}\right]$	$\frac{k}{4}\left[(D_i^n+D_{i-1}^n)\,\frac{c_i^n-c_{i-1}^n}{x_i^n-x_{i-1}^n}+(D_i^{n+1}+D_{i-1}^{n+1})\,\frac{c_i^{n+1}-c_{i-1}^{n+1}}{x_i^{n+1}-x_{i-1}^{n+1}}\right.$ $\left.-(D_{i+1}^n+D_i^n)\frac{c_{i+1}^n-c_i^n}{x_{i+1}^n-x_i^n}-(D_{i+1}^{n+1}+D_i^{n+1})\,\frac{c_{i+1}^{n+1}-c_i^{n+1}}{x_{i+1}^{n+1}-x_i^{n+1}}\right]$	$\frac{k}{4}\left[(D_{I-1}^n+D_{I-2}^n)\,\frac{c_{I-1}^n-c_{I-2}^n}{x_{I-1}^n-x_{I-2}^n}\right.$ $\left.+(D_{I-1}^{n+1}+D_{I-2}^{n+1})\,\frac{c_{I-1}^{n+1}-c_{I-2}^{n+1}}{x_{I-1}^{n+1}-x_{I-2}^{n+1}}\right]$
$A_i\left(u\hat{c}\,\frac{\partial\phi^{(i)}}{\partial x}\right)$	$-\frac{k}{4}(u_1^n c_1^n+u_1^{n+1}c_1^{n+1}$ $+u_2^n c_2^n+u_2^{n+1}c_2^{n+1})$	$\frac{k}{4}(u_{i-1}^n c_{i-1}^n+u_{i-1}^{n+1}c_{i-1}^{n+1}-u_{i+1}^n c_{i+1}^n-u_{i+1}^{n+1}c_{i+1}^{n+1})$	$\frac{k}{4}(u_{I-2}^n c_{I-2}^n+u_{I-2}^{n+1}c_{I-2}^{n+1}$ $+u_{i-1}^n c_{i-1}^n+u_{i-1}^{n+1}c_{i-1}^{n+1})$
$A_i(q\hat{c}\,\phi^{(i)})$	$\frac{k}{6}(q_1^n c_1^n+q_0^{n+1}c_0^{n+1}$ $+q_1^{n+1}c_1^{n+1})(x_1^{n+1}-x_0^{n+1})$ $+\frac{k}{4}[(x_2^n-x_1^n)q_1^n c_1^n$ $(x_2^{n+1}-x_1^{n+1})q_1^{n+1}c_1^{n+1}]$	$\frac{k}{4}[(x_{i+1}^n-x_{i-1}^n)q_i^n c_i^n+(x_{i+1}^{n+1}-x_{i-1}^{n+1})q_i^{n+1}c_i^{n+1}]$	$\frac{k}{4}[(x_I^n-x_{I-2}^n)q_{I-1}^n c_{I-1}^n$ $+(x_I^{n+1}-x_{I-2}^{n+1})q_{I-1}^{n+1}c_{I-1}^{n+1}$ $+(x_I^n-x_{I-1}^n)q_I^n c_I^n$ $+(x_I^{n+1}-x_{I-1}^{n+1})q_I^{n+1}c_I^{n+1}]$
$L_{n+1,i-1}(s\hat{c}\,\phi^{(i)})$ $+L_{n+1,i}(s\hat{c}\,\phi^{(i)})$	$\frac{1}{2}[(x_1^{n+1}-x_0^{n+1})s_0^{n+1}c_0^{n+1}$ $+(x_2^{n+1}-x_0^{n+1})s_1^{n+1}c_1^{n+1}]$	$\frac{1}{2}(x_{i+1}^{n+1}-x_{i-1}^{n+1})s_i^{n+1}c_i^{n+1}$	$\frac{1}{2}[(x_I^{n+1}-x_{I-2}^{n+1})s_{I-1}^{n+1}c_{I-1}^{n+1}$ $+(x_I^{n+1}-x_{I-1}^{n+1})s_I^{n+1}c_I^{n+1}]$
$L_{n,i-1}(s\hat{c}\,\phi^{(i)})$ $+L_{n,i}(s\hat{c}\,\phi^{(i)})$	$\frac{1}{2}(x_2^n-x_1^n)s_1^n c_1^n$	$\frac{1}{2}(x_{i+1}^n-x_{i-1}^n)s_i^n c_i^n$	$\frac{1}{2}[(x_I^n-x_{I-2}^n)s_{I-1}^n c_{I-1}^n$ $+(x_I^n-x_{I-1}^n)s_I^n c_I^n$

TABLE II

$L_{x_L}\left(D\frac{\partial \hat{c}}{\partial x}\phi^{(1)}\right)$	$\frac{1}{2}k\,(D_0^{n+1}+D_1^{n})\frac{c_1^{n+1}-c_0^{n+1}}{x_1^{n+1}-x_0^{n+1}}$
$L_{x_L}(u\hat{c}\,\phi^{(1)})$	$\frac{1}{2}k\,(u_1^{n}c_1^{n}+u_0^{n+1}c_0^{n+1})$
$L_{x_R}\left(D\frac{\partial \hat{c}}{\partial x}\phi^{(I-1)}\right)$	$\frac{1}{2}k\left(D_I^{n+1}\frac{c_I^{n+1}-c_{I-1}^{n+1}}{x_I^{n+1}-x_{I-1}^{n+1}}+D_I^{n}\frac{c_I^{n}-c_{I-1}^{n}}{x_I^{n}-x_{I-1}^{n}}\right)$
$L_{x_R}(u\hat{c}\,\phi^{(I-1)})$	$\frac{1}{2}k\,(u_I^{n+1}c_I^{n+1}+u_I^{n}c_I^{n})$

istic base curve passing through the point $P_j^n(x_j^n, t^n)$ of the finite element mesh can be obtained by integrating the first two equations of Eq. (30) to yield

$$\int_{P_j^n}^{\bar{P}_j^{n+1}} s(x)\,dx = \int_{P_j^n}^{\bar{P}_j^{n+1}} u(x,t)\,dt \tag{31}$$

where the point $\bar{P}_j^{n+1}(\bar{x}_j^{n+1}, t^{n+1})$ is a point on the characteristic curve passing through P_j^n. Similarly, the last two equations of Eq. (30) yield

$$\int_{P_j^n}^{\bar{P}_j^{n+1}} \frac{dt}{s(x)} = -\int_{P_j^n}^{\bar{P}_j^{n+1}} \frac{dC}{[q(x,t)+\partial u/\partial x]C}. \tag{32}$$

Employing the mean value theorem for integrals (Clark [5]), Eqs. (31), (32) can be written as

$$s(\tilde{P}_j)(\bar{x}_j^{n+1}-x_j^{n}) = ku(\tilde{\tilde{P}}_j), \tag{33}$$

$$-k\left[q(\tilde{P}_j^{*})+\frac{\partial u}{\partial x}(\tilde{P}_j^{*})\right]C(\tilde{P}_j^{*}) = s(\tilde{\tilde{P}}_j^{*})[C(\bar{P}_j^{n+1})-C(P_j^{n})] \tag{34}$$

in which $\tilde{P}_j$, $\tilde{\tilde{P}}_j$, $\tilde{P}_j^{*}$, $\tilde{\tilde{P}}_j^{*}$ are points on the characteristics curve joining $\bar{P}_j^{n+1}$ and P_j^n. The characteristic passing through P_j^n and $\bar{P}_j^{n+1}$ (Eq. (33)) will be approximated by

$$s_j^{n}(\bar{x}_j^{n+1}-x_j^{n}) = ku_j^{n} \tag{35}$$

which is obtained from Eq. (33) by first expanding $S(\tilde{P}_j)$ and $u(\tilde{\tilde{P}}_j)$ about the point P_j^n in Taylor series and neglecting terms of higher order than $|\bar{x}_j^{n+1}-x_j^{n}|$ and k.

The finite element formulation developed in the previous section has no restrictions on the orientation of the sides $P_i^nP_i^{n+1}$ $(i = 1,\ldots, I-1)$ of the finite elements. Suppose P_j^{n+1} in the finite element mesh is chosen such that $x_j^{n+1} = \bar{x}_j^{n+1}$ where $\bar{x}_j^{n+1}$ is evaluated from Eq. (35). This is equivalent to choosing the line segment which is a first order approximation to characteristic passing through P_j^n as the side $P_j^nP_j^{n+1}$ in the finite element mesh. Now, it is possible to check if the finite element solution technique is

proper in the limiting case $D = 0$, by comparing c_j^{n+1} obtained from the finite element equations (Eq. (20) for which each term is given explicitly in Tables I and II) with the solution obtained employing characteristics given by Eq. (34). This comparison shows that if not only P_j^{n+1} but all the nodes at $t = t^{n+1}$ are chosen such that

$$s_i^n(x_i^{n+1} - x_i^n) = ku_i^n, \qquad i = 1, 2,..., I-1, \tag{36}$$

the finite element equations for $D = 0$ yield a first order approximation in $| x_i^{n+1} - x_i^n |$ and k of (34) for $j = 1, 2,..., I-1$. Thus, the linear system of equations obtained from finite elements by constraining the orientation of the sides $P_i^n P_i^{n+1}$ ($i = 1, 2,..., I-1$) of the finite elements according to Eq. (36) yields

$$\begin{aligned}
&\frac{1}{4}[ku_1^{n+1} - (x_1^{n+1} - x_1^n)\, s_1^{n+1} + 2(x_2^{n+1} - x_0^{n+1})\, s_1^{n+1}]\, c_1^{n+1} \\
&\quad + \frac{1}{4}[ku_2^{n+1} - (x_2^{n+1} - x_2^n)\, s_2^{n+1}]\, c_2^{n+1} - \frac{1}{2}[ku_1^n + (x_2^n - x_1^n)\, s_1^n]\, c_1^n \\
&\quad - \frac{1}{2}[ku_0^{n+1} - (x_1^{n+1} - x_0^{n+1})\, s_0^{n+1}]\, c_0^{n+1} \\
&\quad - \frac{k}{4}\left[(D_1^n + D_2^n)\frac{c_2^n - c_1^n}{x_2^n - x_1^n} + (D_1^{n+1} + D_2^{n+1})\frac{c_2^{n+1} - c_1^{n+1}}{x_2^{n+1} - x_1^{n+1}}\right. \\
&\quad \left. - 2(D_0^{n+1} + D_1^n)\frac{c_1^{n+1} - c_0^{n+1}}{x_1^{n+1} - x_0^{n+1}}\right] + \frac{k}{4}\left[(x_2^n - x_1^n)q_1^n c_1^n + (x_2^{n+1} - x_1^{n+1})q_1^{n+1}c_1^{n+1}\right. \\
&\quad \left. + \frac{2}{3}(x_1^{n+1} - x_0^{n+1})(q_1^n c_1^n + q_0^{n+1}c_0^{n+1} + q_1^{n+1}c_1^{n+1})\right] = 0,
\end{aligned} \tag{37}$$

$$\begin{aligned}
&\frac{1}{4}[ku_{i+1}^{n+1} - (x_{i+1}^{n+1} - x_{i+1}^n)\, s_{i+1}^{n+1}]\, c_{i+1}^{n+1} - \frac{1}{4}[ku_{i-1}^{n+1} - (x_{i-1}^{n+1} - x_{i-1}^n)\, s_{i-1}^{n+1}]\, c_{i-1}^{n+1} \\
&\quad + \frac{1}{2}[(x_{i+1}^{n+1} - x_{i-1}^{n+1})\, s_i^{n+1} c_i^{n+1} - (x_{i+1}^n - x_{i-1}^n)\, s_i^n c_i^n] \\
&\quad - \frac{k}{4}\left[(D_i^n + D_{i+1}^n)\frac{c_{i+1}^n - c_i^n}{x_{i+1}^n - x_i^n} - (D_i^n + D_{i-1}^n)\frac{c_i^n - c_{i-1}^n}{x_i^n - x_{i-1}^n}\right. \\
&\quad \left. + (D_{i+1}^{n+1} + D_i^{n+1})\frac{c_{i+1}^{n+1} - c_i^{n+1}}{x_{i+1}^{n+1} - x_i^{n+1}} - (D_i^{n+1} + D_{i-1}^{n+1})\frac{c_i^{n+1} - c_{i-1}^{n+1}}{x_i^{n+1} - x_{i-1}^{n+1}}\right] \\
&\quad + \frac{k}{4}[(x_{i+1}^n - x_{i-1}^n)\, q_i^n c_i^n + (x_{i+1}^{n+1} - x_{i-1}^{n+1})\, q_i^{n+1} c_i^{n+1}] = 0, \qquad i = 2, 3,..., I-2,
\end{aligned} \tag{38}$$

$$\begin{aligned}
&-\frac{1}{4}[ku_{I-2}^{n+1} - (x_{I-2}^{n+1} - x_{I-2}^n)\, s_{I-2}^{n+1}]\, c_{I-2}^{n+1} + \frac{1}{2}[ku_I^{n+1} + (x_I^{n+1} - x_{I-1}^{n+1})\, s_I^{n+1}]\, c_I^{n+1} \\
&\quad + \frac{1}{2}[ku_I^n - (x_I^n - x_{I-1}^n)\, s_I^n]\, c_I^n + \frac{1}{4}[-ku_{I-1}^{n+1} + (x_{I-1}^{n+1} - x_{I-1}^n)\, s_{I-1}^{n+1}
\end{aligned}$$

$$+ 2(x_I^{n+1} - x_{I-2}^{n+1})\, s_{I-1}^{n+1}]\, c_{I-1}^{n+1} - \frac{1}{2}(x_I^n - x_{I-2}^n)\, s_{I-1}^n c_{I-1}^n$$

$$+ \frac{k}{4}\left[(D_{I-1}^n + D_{I-2}^n)\frac{c_{I-1}^n - c_{I-2}^n}{x_{-1}^n - x_{I-2}^n} + (D_{I-1}^{n+1} + D_{I-2}^{n+1})\frac{c_{I-1}^{n+1} - c_{I-2}^{n+1}}{x_{I-1}^{n+1} - x_{I-2}^{n+1}}\right.$$

$$\left. - 2D_I^{n+1}\frac{c_I^{n+1} - c_{I-1}^{n+1}}{x_I^{n+1} - x_{I-1}^{n+1}} - 2D_I^n\frac{c_I^n - c_{I-1}^n}{x_I^n - x_{I-1}^n}\right] + \frac{k}{4}[(x_I^n - x_{I-2}^n)\, q_{I-1}^n c_{I-1}^n$$

$$+ (x_I^{n+1} - x_{I-2}^{n+1})\, q_{I-1}^{n+1} c_{I-1}^{n+1} + (x_I^n - x_{I-1}^n)\, q_I^n c_I^n + (x_I^{n+1} - x_{I-1}^{n+1})\, q_I^{n+1} c_I^{n+1}] = 0. \tag{39}$$

These $I - 1$ equations in unknowns c_i^{n+1} $(i = 1, 2,..., I - 1)$ are obtained by writing Eq. (20) explicitly and employing Tables I and II together with Eq. (36). Here, $x_1^n = x_0^{n+1} = x_L$ and $x_I^n = x_I^{n+1} = x_R$. A space–time mesh with nodes x_i^n $(i = 2,..., I - 1)$ and x_i^{n+1} $(i = 1, 2,..., I - 1)$ varying in time is generated at each time step employing Eq. (36). The details of the automatic mesh generation are given in Section 5.

Now it should be clear that if $u(x_L, t) > 0$ and $u(x_R, t) > 0$ the characteristic passing through x_1^n enters, and the characteristics passing through x_I^n leaves the region $x_L \leqslant x \leqslant x_R$. Therefore, if the finite element mesh is to be oriented along with characteristics, a triangular element is required next to the left hand boundary to account properly for the effect of the boundary condition at the left hand boundary, especially in the case of convection dominated transport.

In the case of pure diffusion $(u(x, t) = 0)$, $P_1^{n+1} = P_0^{n+1}$ and the triangular element K_0^n vanishes and the unknowns of the problem, c_i^{n+1} $(i = 2, 3,..., I - 1)$, can be evaluated from Eqs. (38), (39) using $u_i^n = u_i^{n+1} = 0$ $(i = 1,..., I - 1)$.

In the case of pure convection $D = 0$, the boundary condition at $x = x_R$ is redundant (for $u(x_R, t) > 0$) and the unknowns can be evaluated from Eqs. (37), (38) where Eq. (38) now applies for $i = 2, 3,..., I - 1$. The righthand boundary is no longer fixed and x_I^{n+1} will be evaluated from Eq. (36) by substituting $i = I$. It is possible to choose x_I^0 sufficiently large (in the case of $u(x_I^n, t^n) > 0$) so that $c_I^n = 0$ for the time interval $0 \leqslant t^n < T$ for which solution is sought.

In the case of constant coefficients $u(x, t) =$ constant, $s(x) =$ constant, the characteristics are straight lines and the finite element method yields the exact solution in pure convection with $q(x, t) = 0$.

3.4. *Other Boundary Conditions*

If boundary conditions are given as

$$\frac{\partial C}{\partial x}(x_L, t) = \bar{c}_L(t), \qquad t > 0, \tag{40}$$

$$\frac{\partial C}{\partial x}(x_R, t) = \bar{c}_R(t), \qquad t > 0 \tag{41}$$

instead of Eqs. (3), (4), the nodal values of the approximating function $\hat{c}$ on the boundaries (c_0^{n+1} and c_I^{n+1}) must be evaluated in addition to unknowns c_i^{n+1}, $i = 1, 2,..., I-1$. Weighting function $\phi(x, t)$ must be taken for each i ($i = 0, 1, 2,..., I$) as

$$\begin{aligned} \bar{\phi}^{(i)}(P_j^{n+1}) &= 1, \quad i = j \\ &= 0, \quad i \neq j \end{aligned} \qquad j = 0, 1,..., I$$

$$\begin{aligned} \bar{\phi}^{(i)}(P_j^{n}) &= 1, \quad i = j \\ &= 0, \quad i \neq j \end{aligned} \qquad j = 1, 2,..., I$$

$$i = 0, 1,..., I \tag{42}$$

Then $I + 1$ weighted residual equations are obtained replacing $\phi^{(i)}$ by $\bar{\phi}^{(i)}$ in Eq. (20) and noting that for this case, $i = 0, 1,..., I$. In view of Eq. (42), we have

$$\sum_{i=0}^{I} \bar{\phi}^{(i)} = 1, \qquad x_L \leqslant x \leqslant x_R, \qquad t^n \leqslant t \leqslant t^{n+1} \tag{43}$$

and therefore Eq. (22) is also valid in this case. The system of $(I + 1)$ linear equations in unknowns $c_0^{n+1},..., c_I^{n+1}$ can be obtained by evaluating finite element contributions to the modified form of Eq. (20), as explained before, and orienting the sides of the finite elements joining the nodes $P_i^n P_i^{n+1}$ such that Eq. (36) is satisfied. It should be noted that

$$\bar{\phi}^{(i)} = \phi^{(i)} \qquad i = 2, 3,..., I-2 \tag{44}$$

and therefore for the new boundary conditions, Eq. (38) is valid for $i = 2, 3,..., I-2$. The new form of the equations for $i = 0, 1$ and $I-1, I$ will not be given here explicitly to avoid more lengthy expressions; they are readily derivable.

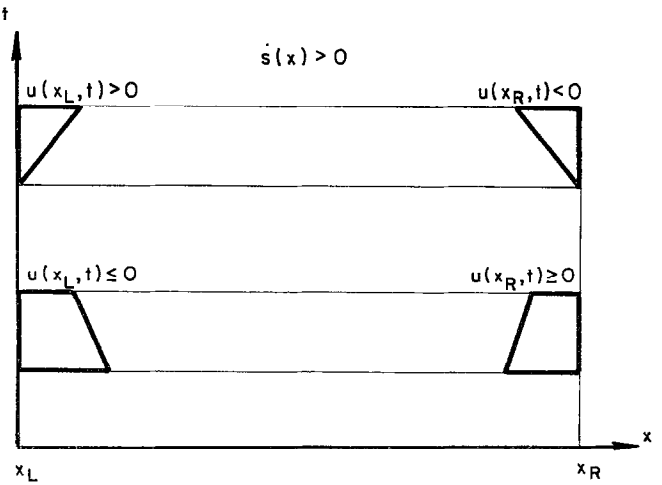

FIG. 2. Velocity field and type of elements to be used next to the boundaries.

3.5. *Effect of the Boundary Values of the Velocity Field*

So far, the method has been developed assuming that $u(x_L, t) > 0$ and $u(x_R, t) > 0$ for $t > 0$. This assumption was necessary in order to give the system of linear equations (Eqs. (37)–(39)) for a concrete case. The boundary values of the velocity field determine whether or not the characteristics of the associated equation, Eq. (29), at x_1^n and x_I^n enter the region $x_L \leqslant x \leqslant x_R$ at a typical time step. If at a typical time step, a characteristic at x_1^n or x_I^n enters the region $x_L \leqslant x \leqslant x_R$ the finite element mesh should contain a triangular element next to that boundary as shown in Fig. 2. Since the finite element equations are developed by first evaluating the triangular and trapezoidal element contributions as given in Table I, this table can be used with slight modifications to evaluate the contributions from trapezoidal and triangular elements to the weighted residual equations for any combination of the left and right boundary values of the velocity field at each time step.

4. Examples

The numerical results for three problems are given using the finite element method incorporating characteristics (FEMIC) developed in the previous sections. The coefficients and other parameters used in these problems are summarized in Table III.

TABLE III

Problem no.	$s(x)$	$D(x, t)$	$u(x, t)$	$q(x, t)$	x_L	x_R
1	1	1	$-1/x$	$-1/x^2$	0.5	2.50
2	$1-0.5x$	$(2-x)\times 10^{-6}$	0.0004	0	0	1
3	1	1	10^4	0	0	1

Problem 1 is supplemented with the boundary conditions

$$\begin{aligned} \bar{c}_L(t) &= \frac{\partial C}{\partial x}(x_L, t) = -\frac{2}{x_L}\exp(-x_L^2/4t), \\ c_R(t) &= C(x_R, t) = -Ei(-x_R^2/4t) \end{aligned} \tag{45}$$

and the initial condition

$$C(x, 0) = 0. \tag{46}$$

Here, Ei denotes exponential integral expressed as

$$Ei(-u) = -\int_u^\infty (e^{-v}/v)\, dv. \tag{47}$$

This problem has an exact solution

$$C(x, t) = -Ei(-x^2/4t), \qquad x_L \leqslant x \leqslant x_R, \qquad t > 0 \tag{48}$$

which can be verified by direct substitution into the differential equation and the auxiliary conditions. The comparison of the results from FEMIC with the exact solution is illustrated in Fig. 3 for $t = 0.10$, 0.50, 1.00 and 2.00. Two time steps $\Delta t = 0.05$ and $\Delta t = 0.10$ are employed to demonstrate convergence properties of the numerical solution and to give an indication of the stability and accuracy obtained by reasonable time step sizes. Initially, the interval $0.5 \leqslant x \leqslant 2.5$ is discretized by 50 equally spaced nodes for both of the time steps. The agreement between the exact solution and the numerical solution for $\Delta t = 0.05$ is very good.

Problem 2 is related to the propagation of a concentration front through a channel with cross-sectional area varying linearly with distance from $x_L = 0$ (Dailey and Harleman [6]). The auxiliary conditions are taken as

$$\begin{aligned} c_L(t) &= C(0, t) = 1, \\ c_R(t) &= C(1, t) = 0, \\ C(x, 0) &= 0. \end{aligned} \tag{49}$$

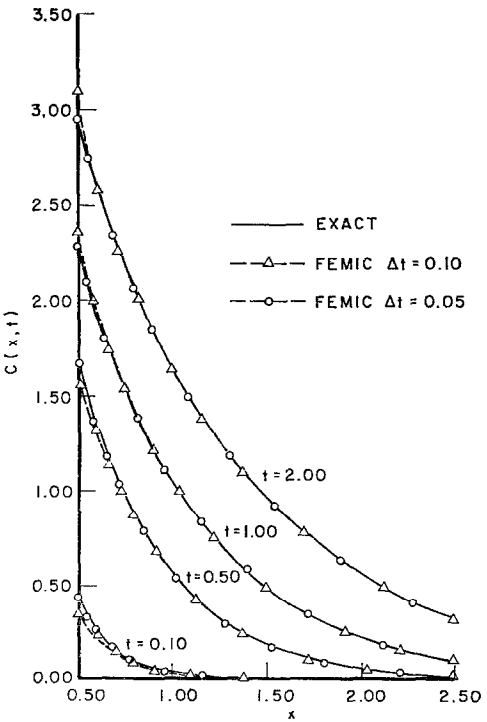

FIG. 3. Problem 1, Comparison of numerical solution from FEMIC and exact solution.

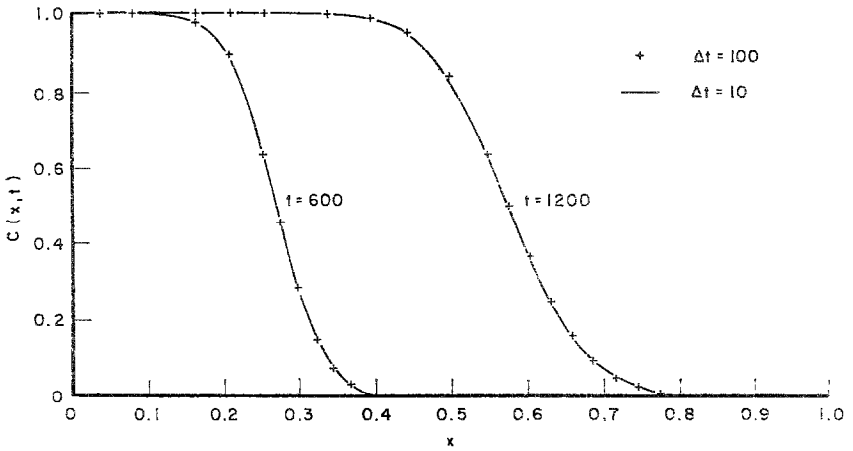

FIG. 4. Problem 2, Numerical solution from FEMIC.

Results from FEMIC for $t = 600$ and $t = 1200$ are illustrated in Fig. 4. Initially, the interval $0 \leqslant x \leqslant 1$ is discretized by 50 equally spaced nodes. The numerical results for $\Delta t = 10$ and $\Delta t = 100$ are in good agreement with each other.

Problem 3 is solved for the initial rectangular wave given as

$$\begin{aligned} C(x, 0) &= 1, \quad 0.095 < x < 0.205, \\ &= 0, \quad 0 < x < 0.095, \quad 0.205 < x < 1 \end{aligned} \tag{50}$$

and the boundary conditions

$$\begin{aligned} c_L(t) &= C(0, t) = 0, \\ c_R(t) &= C(1, t) = 0. \end{aligned} \tag{51}$$

This is one of the standard test problems utilized by Lam [13] to test the performance of several numerical techniques for highly convection dominated flows. The numerical results for standard finite element scheme (FEM), upstream differencing (UDS) and flux-corrected upstream differencing (UDS + FCT) are compared with the exact solution in Lam [13]. This study reveals that the standard FEM solution exhibits oscillations with an amplitude of 15% of the maximum concentration and that an overshoot about 15% higher than the maximum value of the exact concentration appears in the solution. UDS results show considerable numerical diffusion. The most accurate results are obtained from UDS + FCT which exhibit only a small amount of distortion of the symmetry of the concentration profile. The above mentioned solutions are obtained employing $\Delta t = 6 \times 10^{-7}$ and a spatial discretization $\Delta x = 1/100$.

The results from FEMIC are illustrated in Fig. 5 for time steps $\Delta t = 6 \times 10^{-7}$ and $\Delta t = 6 \times 10^{-5}$ employing initially the same spatial discretization employed by

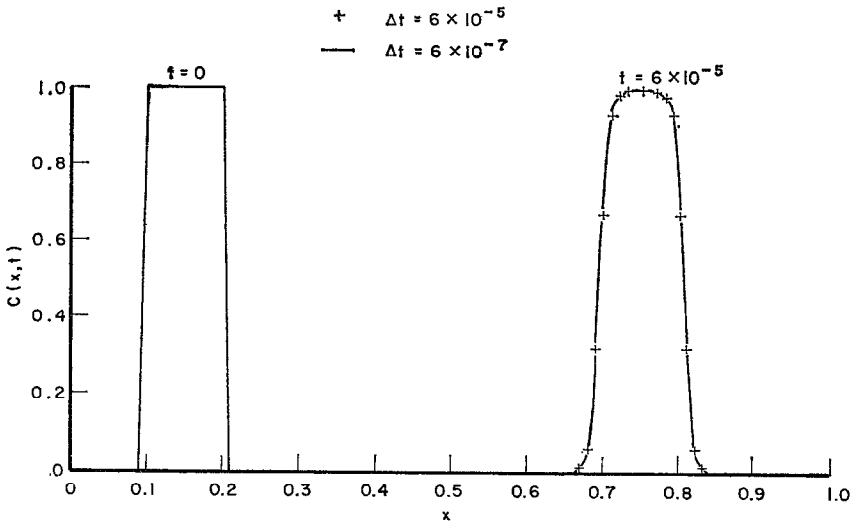

FIG. 5. Problem 3, Rectangular wave at $t = 0$ and solution from FEMIC at $t = 6 \times 10^{-5}$.

Lam [13]. Results from FEMIC are very accurate even for $\Delta t = 6 \times 10^{-5}$. The solution by FEMIC does not exhibit any oscillation, overshoot or distortion of symmetry.

The numerical resluts presented were obtained on an AMDAHL 470 V/6–II computer at the University of British Columbia. The total processing time necessary for the generation of the mesh, and the construction and solution of the resulting system of linear equations at each time step was less than 0.05 sec. for all of the examples.

5. Automatic Mesh Generation

At each time step, a new space–time mesh is automatically generated by the algorithm MESH. The interval $x_L \leqslant x \leqslant x_R$ is initially discretized by I nodes, $x_1^0 = x_L$, $x_2^0, \ldots, x_{I-1}^0$, $x_I^0 = x_R$. These nodes can be equally or variably spaced. The selection of initial discretization is guided by the accuracy desired in the representation of the initial condition and in the evaluation of the solution for $t > 0$. For instance, a fine initial mesh in the interval $0.08 < x < 0.22$ and a coarse mesh outside of this interval is more suitable than a uniform initial mesh to represent the initial rectangular wave form at $0.10 < x < 0.20$ and the resulting solution of problem 3, although results obtained from initially uniform meshes are given in the previous section to simplify presentation, and comparison with the other published results.

The time step size is an important parameter which may be prescribed as constant or variable. The accuracy of the representation of the time dependent boundary conditions and the fineness of the mesh for $t > 0$ is affected by the time step size.

At a typical time step n, the algorithm MESH computes the x-coordinates of the prospective nodes at $t = t^{n+1}$ from Eq. (36) as

$$x_i^{n+1} = x_i^n + ku_i^n/s_i^n, \qquad i = 1, 2,..., I-1. \tag{52}$$

From these nodes, only the ones which satisfy the conditions

$$x_L < x_i^{n+1} < x_R, \qquad i = 1, 2,..., I-1 \tag{53}$$

and

$$x_{i+1}^{n+1} - x_i^{n+1} > 0, \qquad i = 1, 2,..., I-1 \tag{54}$$

are retained in order to automatically generate the time-space mesh for $t^n \leqslant t \leqslant t^{n+1}$ as shown in Fig. 1. The computer program has an option for which computations are terminated if the total number of nodes retained after a number of time steps are either greater than a prescribed upper bound or less than a prescribed lower bound in order to start with a proper number of nodes from this time on, as a new initial-boundary value problem. In the example problems, this option is not used.

It should be noted that some nodes may leave the region $x_L < x < x_R$ at each or some time steps. The use of triangular elements next to the boundary at $x = x_L$ facilitates entrance of one node into the region at each time step. In general, as the time step size decreases, the mesh generated becomes gradually finer with time. Also, by increasing the time step size, the mesh can be made gradually coarser with time. For instance, in problem 1, the total number of nodes initially is 50. At $t = 2$, the total number of nodes is 53 and 32 for $\Delta t = 0.05$ and $\Delta t = 0.01$, respectively. For $\Delta t = 0.10$, nodes are lost at $x = 0.5$ faster than they are replenished at $x = 2.5$. But numerical results clearly show that there is neither an appreciable accuracy loss in the solution nor any difficulty in satisfying the time dependent boundary condition at $x = 0.5$ that could directly be attributed to the loss of nodes faster than they are replenished. The accuracy loss in the case of $\Delta t = 0.10$ in comparison to the results obtained for $\Delta t = 0.05$ is simply a result of having the time step size twice as large (Figure 3).

In problem 2, the initial total number of nodes is also 50. At $t = 1200$, there are 29 and 136 nodes for $\Delta t = 100$ and $\Delta t = 10$, respectively. For $\Delta t = 100$, at each time step a new node is generated with a space increment, $h = u\,\Delta t = 0.04$, which is twice as large as that of the initial space increment. As a result of this, the automatically generated mesh at $t = 1200$ is coarser ($h \simeq 0.04$) in the interval $0 < x < 0.55$ and finer ($h \simeq 0.02$) for $0.55 < x < 1.00$. The numerical results shown in Figure 4 demonstrate that the coarser mesh in the interval, $0 < x < 0.55$, does not cause any numerical difficulty or loss of overall accuracy because of the non-vanishing boundary condition at $x = 0$.

In literature, the time step size for convection dominated flow problems with constant u and s is chosen satisfying the condition

$$\Delta t \leqslant \epsilon(s/u)h \tag{55}$$

where ϵ is a constant between 0.1 and 1 (Ehlig [7], Jamet and Bonnerot [10], Lam [13]) and h is the uniform space increment.

In problem 3, in order to emphasize the capability of the method to work with very large time steps for convection dominated flow problems, the time step is also chosen as $\Delta t = 6 \times 10^{-5}$ ($\epsilon = 60$). At one time step, 60 elements out of 100 of size $h = 0.01$ have left the region $0 < x < 1$, and only one element of size $h = u \cdot \Delta t = 0.60$ is generated next to the boundary at $x = 0$, although the mesh under the rectangular wave is still as fine as it was initially. Since the solution obtained from Eqs. (37), (38) for $q = 0$, $s = 1$, $c_L(t) =$ constant reduces to

$$c_i^n \to c_i^{n+1} \qquad \text{for} \quad x_i^{n+1} = x_i^n + u\,\Delta t, \qquad i = 1, 2, \ldots, \tag{56}$$

in the limiting case of $D/u \to 0$, FEMIC breaks down to the method of characteristics and the numerical solution is exact at nodes, regardless of the time step size for pure convection. Nevertheless, problem 3 is a highly convection dominated flow problem ($D/u = 10^{-4}$) and $c_L(t) =$ constant, therefore, the overall accuracy of the solution at $t = 6 \times 10^{-5}$ obtained employing $\Delta t = 6 \times 10^{-5}$ is the same as that obtained using $\Delta t = 6 \times 10^{-7}$ for all practical purposes, as shown in Fig. 5.

The processing time necessary for the automatic mesh generation is about 5% of the total processing time required to obtain the numerical solution at each time step.

6. Conclusions

A new finite element method (FEMIC) for the solution of the diffusion convection equation with variable coefficients is introduced. The method employs spatial–temporal elements and incorporates the characteristics of the hyperbolic partial differential equation obtained by substituting $D = 0$ into the diffusion convection equation. These characteristics form the sides of the elements joining nodes at consecutive time levels.

The utility and accuracy of the method have been demonstrated by three numerical examples. Numerical results obtained are satisfactory and do not exhibit any oscillations, overshoots or numerical diffusion even for very large time steps. The associated computer program has an algorithm to generate automatically a spatially variable mesh at each time step.

In two-spatial dimensions, the incorporation of the method of characteristics into the finite elements can still be achieved by orienting edges (joining the nodes at subsequent time levels) of the spatial-time finite volume elements along the characteristic lines of the hyperbolic equation obtained by substituting the eddy diffusion coefficients $D_x = D_y = 0$ into the diffusion–convection equation. The development and demonstration of the method for the diffusion–convection equation in two spatial dimensions will be given in a subsequent paper.

ACKNOWLEDGMENTS

Financial assistance under strategic grant No. 67-0215 of the Natural Sciences and Engineering Research Council of Canada is gratefully acknowledged.

REFERENCES

1. R. A. ADEY AND C. A. BREBBIA, *in* "Numerical Methods in Fluid Dynamics" (C. Brebbia and J. J. Connor, Eds.), pp. 325–354, Pentech, London, 1973.
2. R. BONNEROT AND P. JAMET, *Int. J. Num. Meth.* **8** (1974), 811–820.
3. D. L. BOOK, J. P. BORIS, AND K. HAIN, *J. Comput. Phys.* **18** (1975), 248–283.
4. N. M. CHAUDHARI, *Soc. Petrol. Eng. J.* **11**(3), (1971), 277–284.
5. C. CLARK, "The Theoretical Side of Calculus," Wadsworth, Belmont, Calif., 1972.
6. J. E. DAILEY AND D. R. F. HARLEMAN, *in* "Numerical Methods in Fluid Dynamics" (C. Brebbia and J. J. Connor, Eds.), pp. 412–439, Pentech, London, 1973.
7. C. EHLIG, *in* "Finite Elements in Water Resources" (W. G. Gray, G. F. Pinder, and C. A. Brebbia, Eds.), pp. 1.91–1.102, Pentech, London, 1977.
8. W. G. GRAY AND G. F. PINDER, *Water Resour. Res.* **10**(4), (1974), 821–828.
9. F. B. HILDEBRAND, "Advanced Calculus for Engineers," Prentice–Hall, New York, 1954.
10. P. JAMET AND R. BONNEROT, *J. Comput. Phys.* **18** (1975), 21–45.
11. P. JAMET, *in* Séminaire de Mathématiques Supérieures, "Méthodes Numériques en Mathématiques Appliquées," **60**, pp. 102–124, Les Presses de l'Université de Montréal, 1977.
12. H. B. KELLER, "A New Difference Scheme for Parabolic Problems" (B. Hubbard, Ed.), pp. 327–350, Academic Press, New York, 1971.
13. D. C. L. LAM, *in* "Finite Elements in Water Resources" (W. G. Gray, G. F. Pinder, and C. A. Brebbia, Eds.), pp. 1.115–1.129, Pentech, London, 1977.
14. B. MARTIN, *J. Comput. Phys.* **17** (1975), 358–383.
15. J. W. MERCER AND C. R. FAUST, *in* "Finite Elements in Water Resources" (W. G. Gray, G. F. Pinder, and C. A. Brebbia, Eds.), pp. 1.21–1.57, Pentech, London, 1977.
16. J. T. ODEN, "Finite Elements of Nonlinear Continua," McGraw–Hill, New York, 1972.
17. H. S. PRICE, J. C. CAVENDISH, AND R. S. Varga, *Soc. Petrol. Eng. J.* **243**(3), (1968), 293–303.
18. H. S. PRICE, R. S. VARGA, AND J. E. WARREN, *J. Math. Phys.* **45** (1966), 301–311.
19. I. M. SMITH, *in* "Finite Elements in Water Resources" (W. G. Gray, G. F. Pinder, and C. A. Brebbia, Eds.), pp. 1.3–1.20, Pentech, London, 1977.
20. [illegible]
21. M. TH. VAN GENUCHTEN, *in* "Finite Elements in Water Resources" (W. G. Gray, G. F. Pinder, and C. A. Brebbia, Eds.), pp. 1.71–1.90, Pentech, London, 1977.
22. O. C. ZIENKIEWICZ, "The Finite Element Method," 3rd ed., McGraw–Hill, London, 1977.